Comparative study of metal or oxide capped indium–tin oxide anodes for organic light-emitting diodes

Chengfeng Qiu, Zhilang Xie, Haiying Chen, Man Wong,[a] and Hoi Sing Kwok
Center for Display Research, Department of Electrical and Electronic Engineering, The Hong Kong University of Science and Technology, Clear Water Bay, Kowloon, Hong Kong

(Received 21 November 2002; accepted 6 January 2003)

Indium–tin oxide capped with a variety of nanometer-thick metal or oxide buffer layers has been investigated as anodes in organic light-emitting diodes based on *N*,*N*′-diphenyl-*N*,*N*′ bis(3-methyl-phenyl-1,1′-biphenyl-4,4′-diamine/tris-8-hydroxyquinoline aluminum. Although high work-function metal buffer layers led to enhancement in hole-injection efficiency, none of the metals investigated gave rise to improvement in current or power efficiency. On the other hand, diodes with some of the oxide buffer layers exhibited improvement not only in hole injection but also in power efficiency. In particular, when 1 nm thick praseodymium oxide was used as the cap layer, more than double the power efficiency was obtained. © *2003 American Institute of Physics.* [DOI: 10.1063/1.1556184]

I. INTRODUCTION

Organic light-emitting diodes (OLEDs)[1] are challenging liquid crystals as alternative building blocks for flat-panel displays[2] because of their all solid-state nature, faster switching speed, and wider viewing angle. The performance of an OLED is affected not just by the properties of its constituent organic layers but also by the electrodes and their interfaces with charge-transport layers.[3] Recent research efforts have focused on improving the injection and emission efficiency[4] and reliability,[5] and understanding the device physics.[6]

For the injection of electrons, low work-function metals, such as calcium (Ca),[7] magnesium (Mg),[8] and gadolinium (Gd),[9] have been used as cathodes. These metals are highly reactive, hence unstable in air. They are typically capped or alloyed with more stable metals such as aluminum (Al), silver (Ag), etc. Examples of composite cathodes are Ca/Al, Mg/Ag, Mg/MgAg, and Gd/Al.[9,10] Alternatively, ultrathin insulating compounds that contain low work-function metals have been used to allow favorable dipole- or bias-induced realignment of the Fermi levels of the metals and the lowest-unoccupied molecular orbital (LUMO) energy levels of the electron-transport layers. The barrier against electron injection is subsequently reduced. Examples of these are lithium fluoride (LiF) and cesium fluoride.[11,12]

For the injection of holes, indium–tin oxide (ITO) has been widely used as an anode because of its transparency, low resistivity, and high workfunction. ITO with surface-adsorbed hydrocarbon has been found to have reduced injection efficiency.[13] Oxygen plasma[14] or ultraviolet (UV)/ozone (O_3) (Ref. 13) treatment has been applied to remove adsorbed hydrocarbon. In addition, organic anode buffer layers (ABLs) such as copper (II) phthalocyanine (CuPc) (Ref. 15) with suitable highest-occupied molecular orbital (HOMO) energy levels, high work-function metals[16] and transparent insulating oxides[17,18] have been used to enhance injection efficiencies. While surface treatment of ITO increases not only hole injection but also the effective quantum and power efficiency,[13,14] improvement only in hole injection but not in power efficiencies has been reported for high work-function metals deposited on ITO.[16] This clearly implies reduced effective quantum efficiencies, perhaps due to metal contaminant induced quenching of electroluminescence. Furthermore, such metals are only semitransparent, hence they diminish the potential gain in efficiency resulting from their high workfunction.

In this work, the relative performance of OLEDs with anodes consisting of ITO capped with a variety of nanometer-thick metals and oxides was compared. *N*,*N*′-diphenyl-*N*,*N*′ bis(3-methyl-phenyl-1,1′-biphenyl-4,4′-diamine (TPD) and tris-8-hydroxyquinoline aluminum (Alq_3) were used as the respective hole-transport and electron-transport/emission layers. The diode structure was CuPc/TPD/Alq_3, since the use of CuPc has been shown to improve device reliability.[15] The candidate metals were platinum (Pt), nickel (Ni), gold (Au), tin (Sn), lead (Pb), and magnesium (Mg). The candidate oxides were those of praseodymium (Pr_2O_3), yttrium (Y_2O_3), terbium (Tb_4O_7), titanium (TiO_2), zinc (ZnO), niobium (Nb_2O_5), gallium (Ga_2O_3), and tin (SnO_2). It was verified that high work-function metal ABLs enhanced only hole injection but not the power efficiency. On the other hand, certain species of oxide ABLs enhanced not only hole injection but also the quantum and power efficiencies. In particular, the power efficiencies of OLEDs with ITO capped by ~1 nm thick Pr_2O_3 or Y_2O_3 were, respectively, 2.5 and 2 times that of reference diodes with bare ITO anodes.

II. EXPERIMENT

The starting substrates were commercial-grade glass coated with 70 nm thick, 30 Ω ITO. The sequence of precleaning prior to loading into the evaporation chamber consisted of ultrasonic soaking in detergent for 30 min, ultra-

[a]Corresponding author; electronic mail: eemwong@ee.ust.hk

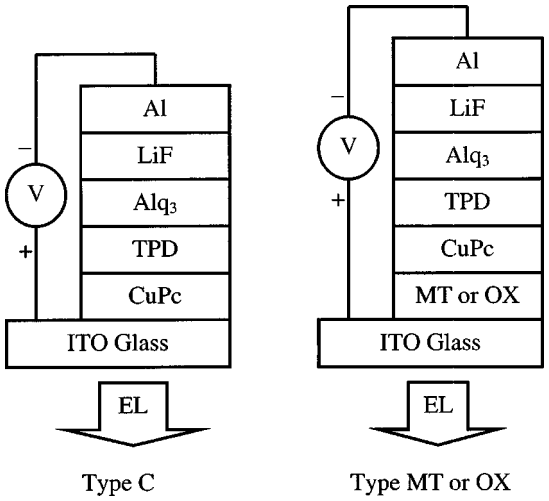

FIG. 1. Schematics of type C, MT, and OX diodes.

sonic soaking in de-ionized (DI) water for 30 min, oven bake drying for 1–2 h, and UV/O_3 illumination for 9 min.[19]

The nanometer-thick metal and oxide cap layers were evaporated using 99.99% pure powder loaded in resistively heated evaporation cells. The deposition rates of the various oxides were between 0.01 and 0.03 nm/s. After evaporation, all samples were subjected to another round of DI water rinsing and UV/O_3 exposure.

The constituent organic layers were next deposited using thermal vacuum evaporation of commercial grade CuPc, TPD, and Alq_3 powder. The base pressure in the evaporator was ~8 μTorr. The deposition rates of the organic thin films were between 0.2 and 0.4 nm/s. While ITO with or without the capped layers formed the anodes, 1 nm LiF topped with 150 nm Al was used for the composite cathodes. The deposition rates of LiF and Al were 0.02–0.05 and 1–1.5 nm/s, respectively. The film thickness was determined *in situ* using a crystal monitor.

Three types of 4 mm diam OLEDs (Fig. 1) were fabricated using a set of shadow masks: type C: ITO (75 nm)/CuPc (20 nm)/TPD (40 nm)/Alq_3 (50 nm)/LiF (1 nm)/Al (150 nm), type MT: ITO/metal (1 nm)/CuPc/TPD/Alq_3/LiF/Al, and type OX: ITO/oxide (1 nm)/CuPc/TPD/Alq_3/LiF/Al.

Unless specified otherwise, the thickness of the various films in types MT and OX diodes was the same as those of the corresponding films in the type C control diode.

The performance of the type C diodes with bare ITO anodes was compared to that of types MT and OX diodes. The diodes were characterized in room ambient and temperature without encapsulation. Photometric characteristics were measured using a Kollmorgen Instruments PR650 photospectrometer. Current–voltage characteristics were measured using a Hewlett-Packard HP4145B semiconductor parameter analyzer.

III. MT TYPE DIODE

The current density–voltage (JV) and luminance–voltage (LV) characteristics of type MT diodes are shown in Figs. 2 and 3, respectively. Compared to the characteristics

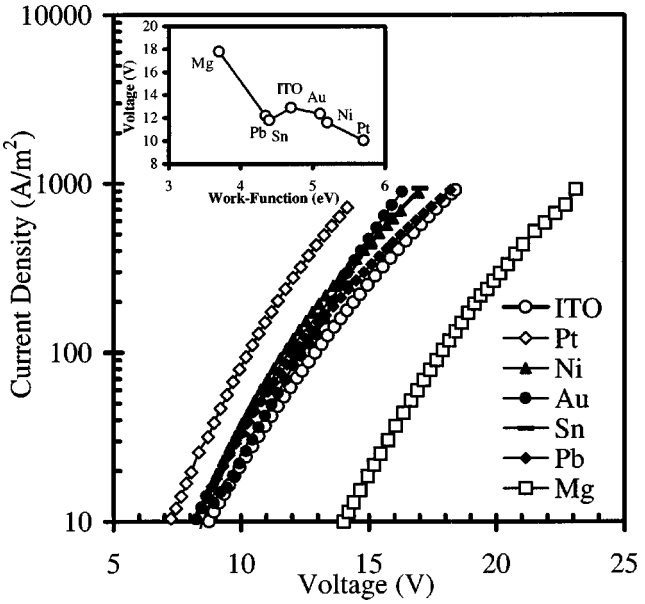

FIG. 2. Current density–voltage characteristics of type C and MT diodes. Shown in the inset is the workfunction dependence of the voltage needed to drive a current density of 100 A/m^2.

of the type C diode with uncapped ITO and depending on the choice of capping metal, both higher and lower driving voltage (V) was obtained for a given J or L. Also shown in the inset of Fig. 2 is the correlation between the V required to achieve $J=100$ A/m^2 and the workfunction[20] of the metal. It is not entirely surprising that a higher workfunction generally leads to a correspondingly lower V.

The dependence of V (hence shifting of the JV or LV curves) on the workfunction of the metal cap can be explained in terms of the energy band alignment diagram shown in Fig. 4. For a type C diode, holes are injected directly into CuPc from ITO. The corresponding "reference" energy barrier is denoted by E_{bi} in Fig. 4(a). With the introduction of a metal cap, a smaller barrier E_b against hole

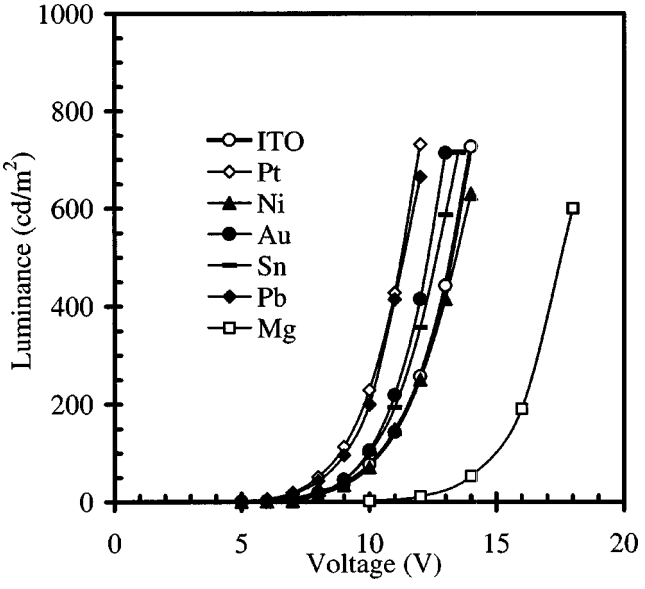

FIG. 3. Luminance–voltage characteristics of type C and MT diodes.

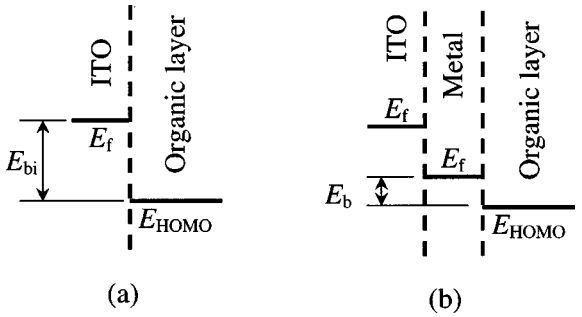

FIG. 4. Energy band alignment diagrams (a) without and (b) with a metal cap layer.

injection [Fig. 4(b)] is obtained for a metal with a workfunction higher than that of ITO. Consequently, a smaller V is required to achieve a given J or L. If a metal, such as Mg, with a lower workfunction was used, E_b versus hole injection became correspondingly larger. It should be noted that the correlation is not absolute since injection efficiency is also affected by details of the interface configuration, such as the formation of interface states,[21] dipoles,[22] etc.

The current efficiency (γ), the power efficiency (η), and V are related by[23]

$$\eta = \pi \frac{L}{VJ} = \pi \frac{1}{V}\left(\frac{L}{J}\right) \equiv \pi \frac{\gamma}{V}, \tag{1}$$

where a Lambertian radiation pattern is assumed. It can be inferred that if γ were maintained constant, η at a given J or L should increase for type MT diodes with higher workfunction metal caps.

The current and power efficiencies of type MT diodes are summarized in Table I. Although higher hole-injection efficiencies were obtained for OLEDs with higher workfunction metal caps, the reduction in γ was more overwhelming and resulted in an overall reduction in η. Diffusion of electroluminescence (EL)-quenching metal contaminants into the emission layer is one possible reason for the reduction in γ.

IV. TYPE OX DIODES

The JV and LV characteristics of type OX diodes are compared to those of type C diodes in Figs. 5 and 6, respectively. Reflecting the improved hole-injection efficiency, smaller V values are required to generate a given J (or L) for type OX diodes with Pr_2O_3, Y_2O_3, Tb_4O_7, ZnO, and Nb_2O_5 caps. The lowest V was obtained with Pr_2O_3. For type OX diodes with TiO_2, Ga_2O_3, and SnO_2 caps, reduced hole-injection efficiencies were measured.

TABLE I. Summary of the characteristics of OLEDs with ITO capped with a variety of metal buffer layers. The characteristics of a reference diode with uncapped ITO are given in the first column.

Metal cap	None	Pt	Ni	Au	Sn	Pb	Mg
Current density (A/m^2) at 8 V	20	50	35	30	28	32	1.5
Max current efficiency (cd/A)	3.5	2.7	2.4	2.5	3.0	3.3	3.0
Max power efficiency (lm/W)	1.1	1.0	0.7	0.7	1.0	0.9	0.7

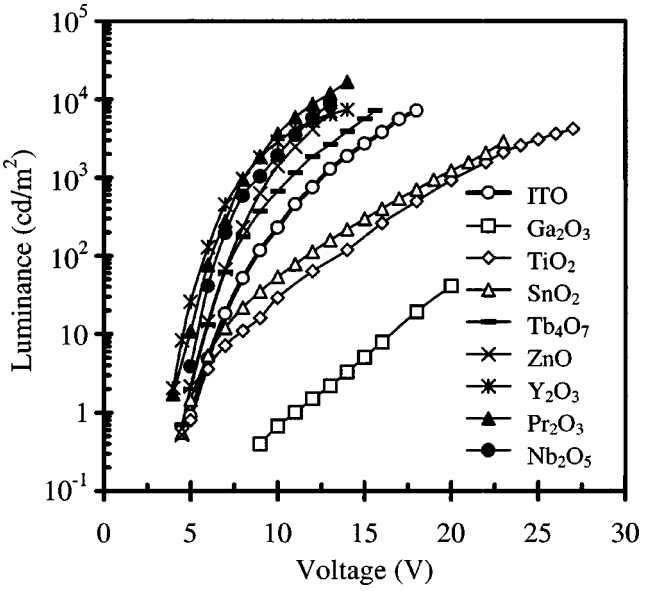

FIG. 5. Luminance–voltage characteristics of type C and OX diodes.

The γJ and ηJ characteristics of the type OX diodes are compared to those of type C diodes in Figs. 7 and 8, respectively. For all diodes, γ initially increases with J, peaks, and then decreases with a further increase in J. Compared to that of a type C diode, γ is larger for type OX diodes with Pr_2O_3, Y_2O_3, Tb_4O_7, ZnO, and Nb_2O_5 caps and decays more gradually beyond the corresponding peak values. For most of the diodes, η decreases with an increase in J. Compared to that of a type C diode, η is improved for type OX diodes with Pr_2O_3, Y_2O_3, Tb_4O_7, ZnO, and Nb_2O_5 caps.

The efficiencies of types OX and C diodes are summarized in Table II. Compared to that of a type C diode, a more than 10 times increase in current injection at a 8 V bias was measured in type OX diodes with Pr_2O_3 or Y_2O_3 caps. On

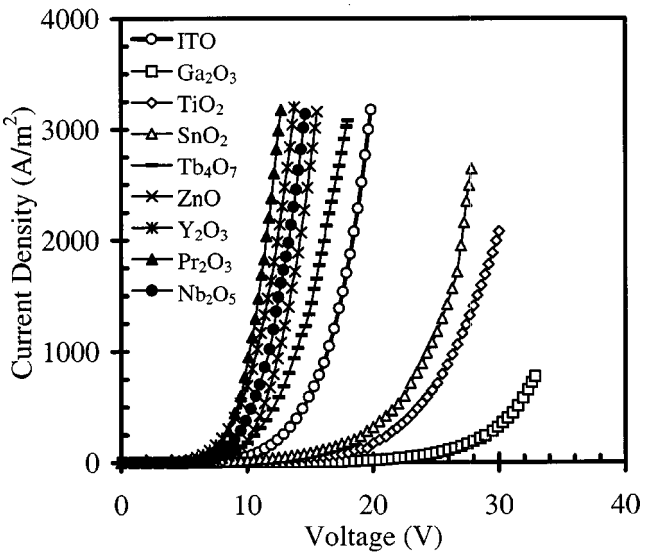

FIG. 6. Current density–voltage characteristics of type C and OX diodes.

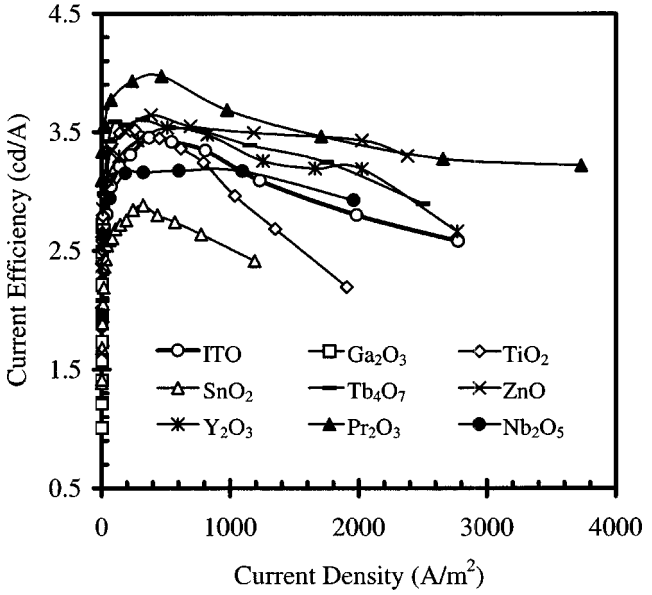

FIG. 7. Current efficiency–current density characteristics of type C and OX diodes.

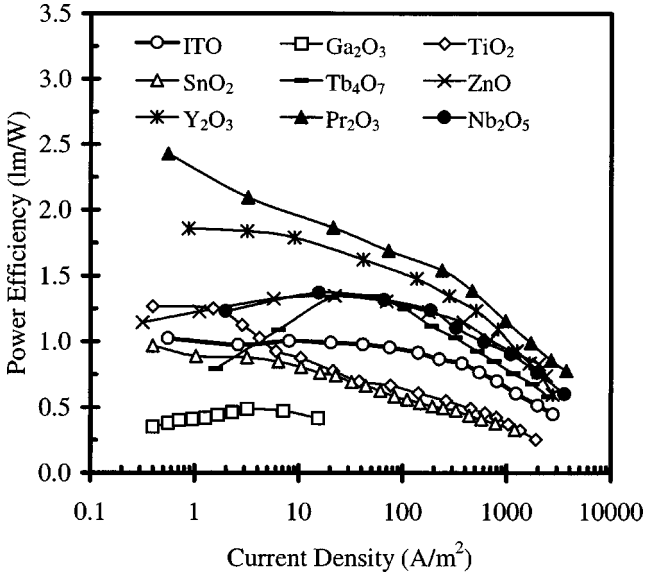

FIG. 8. Power efficiency–current density characteristics of type C and OX diodes.

the contrary, significant reduction in hole injection was measured in diodes with Ga_2O_3 caps. While a peak of $\gamma=2.5$ cd/A was measured for a type C diode, a peak of $\gamma=3.6$ cd/A was obtained at $J=20$ A/m^2 for diodes with Pr_2O_3 caps, representing a ~50% improvement. The largest values of η were measured on diodes with Pr_2O_3 or Y_2O_3 cap layers. They are, respectively, 250% and 200% of the η of a type C diode.

Enhancement of hole-injection efficiency in the presence of an oxide cap can be explained in terms of a reduction of the effective barrier against hole injection from ITO into the organic layer. Without an oxide ABL, hole injection is represented by the arrow against an energy barrier E_{bi} in Fig. 9(a). A positive drop in voltage across the oxide from ITO to the adjacent organic layer could lead to favorable relative displacement of the Fermi level (E_F) of ITO towards the HOMO level (E_{HOMO}) of the organic hole-transport layer [Fig. 9(b)].[24] Consequently, the injection of holes would require overcoming a smaller E_b, followed by tunneling[11,24] [shown by the dashed arrow in Fig. 9(c)] across the thin insulating oxide layer.[25] The drop in voltage across the oxide layer may be induced by a spontaneous electric dipole layer[12] associated with the thin oxide layer, with a portion of the applied bias dropping across the insulating oxide layer or a combination of both.

In principle, any insulator could be used in place of an oxide layer. A given choice of material would be more effective if it possessed a properly aligned spontaneous dipole moment and if it were a better insulator. Pr_2O_3 and Y_2O_3 are good insulators, whereas TiO_2,[26] Ga_2O_3, and SnO_2 are more generally classified as semiconductors with resistivity values neither high enough to sustain the drop in voltage needed to sufficiently reduce E_b nor low enough to function as an efficient hole-transport layer. Consequently, they appear as highly resistive barriers against hole conduction. The supply of holes to the organic hole-transport layer is constrained, thus resulting in degraded hole-injection efficiency. This difference could explain the observed difference among the type OX diodes with different cap oxides.

The ηJ characteristics of the type OX diode with different Pr_2O_3 cap thicknesses are shown in Fig. 10. For a given J, the highest η was measured on diodes with Pr_2O_3 cap thickness of ~1 nm. For a given Pr_2O_3 cap thickness, a peak η can be extracted. Shown in the inset is the dependence on

TABLE II. Summary of the characteristics of OLEDs with ITO capped with a variety of oxides. The characteristics of a reference diode with uncapped ITO are given in the first column.

Oxide cap	None	Ga_2O_3	TiO_2	SnO_2	Tb_4O_7	ZnO	Y_2O_3	Pr_2O_3	Nb_2O_5
Current density (A/m^2) at 8 V	20	0.3	4.2	10.5	50.7	69.9	285	238	180
Current efficiency (cd/m^2) at 20 A/m^2	2.5	2.7	3	2.1	3.0	3.0	3.1	3.6	2.6
Power efficiency (lm/w) at 20 A/m^2	1	0.5	0.7	0.8	1.3	1.3	1.7	1.9	1.4
Max current efficiency (cd/A)	3.5	2.7	3.5	2.9	3.6	3.6	3.7	4.0	3.5
Max power efficiency (lm/w)	1.1	0.5	1.3	1	1.3	1.3	2.0	2.5	1.4

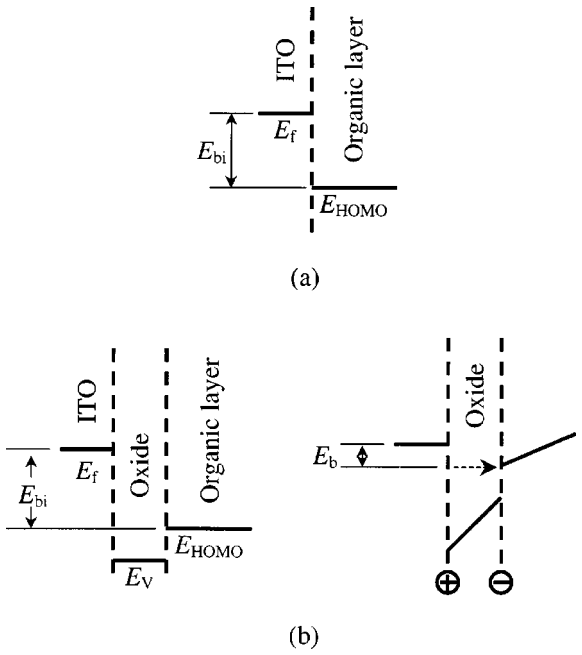

FIG. 9. Energy band diagrams showing how the barrier against hole emission is reduced in the presence of a thin insulating layer. (a) Energy level diagram of a diode with a bare ITO anode. E_{bi} is the energy barrier against emission. (b) Energy level diagram of a diode with an oxide cap. E_v is the valence band level of the oxide layer. Shown on the left is the flatband condition. Shown on the right is bending of the oxide E_v level, induced either by a spontaneous dipole layer or a portion of the bias applied. The bending leads to a reduction in energy barrier E_b, but tunneling across the oxide layer is required.

the cap layer thickness of the relative hole injection and power efficiency of diodes with Pr_2O_3 or Y_2O_3 capped anodes. Relative hole injection and power efficiency are obtained, respectively, by dividing J at a forward bias of 8 V and the peak power efficiency of a diode with a cap by the corresponding values of a type C diode. The initial increase in hole-injection and power efficiencies with Pr_2O_3 or Y_2O_3 thickness could be explained by an increase in Pr_2O_3 or Y_2O_3 coverage. The highest hole-injection and power efficiencies were obtained with Pr_2O_3 or Y_2O_3 thicknesses of $\sim$1 and 1.1 nm, respectively. A subsequent decrease in efficiency beyond the peak values can be explained by the rapidly decreasing tunneling probability across thicker oxide layers.

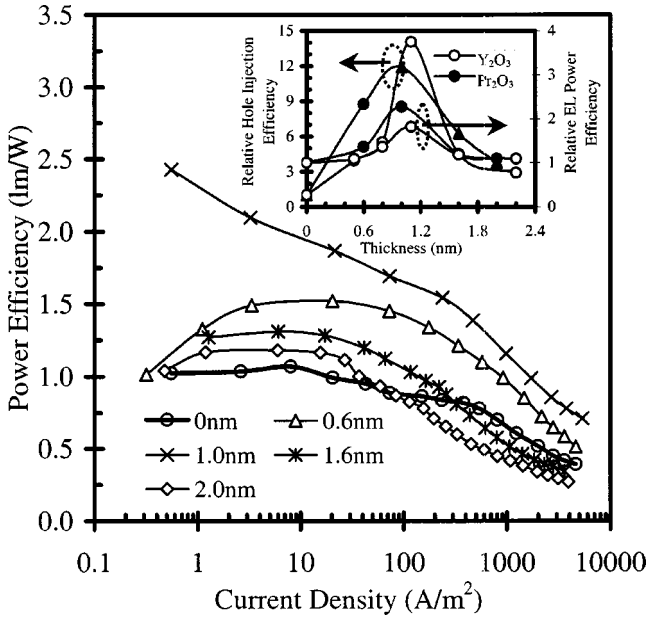

FIG. 10. Power efficiency–current density characteristics of diodes with ITO capped with different thicknesses of Pr_2O_3. Shown in the inset is the dependence on the Pr_2O_3 or Y_2O_3 thickness of the hole injection and power efficiency.

V. CONCLUSION

Indium–tin oxide capped with a variety of nanometer-thick metal (Pt, Ni, Au, Sn, Pb, or Mg) or oxide (Pr_2O_3, Y_2O_3, Tb_4O_7, TiO_2, ZnO, Nb_2O_5, Ga_2O_3 or SnO_2) buffer layers has been investigated as the hole-injecting anodes in CuPc/TPD/Alq_3-based organic light-emitting diodes. Although high work-function metal buffer layers led to enhancement in hole-injection efficiency, none of the metals investigated gave rise to improvement in current or power efficiency. On the other hand, diodes with Pr_2O_3, Y_2O_3, Tb_4O_7, and Nb_2O_5 capped indium–tin oxide anodes exhibited improvement not only in hole injection but also in power efficiency. In particular, an $\sim$10 times increase in hole injection and a more than $\sim$2 times increase in power efficiency have been observed in the case of $\sim$1 nm thick Pr_2O_3 or Y_2O_3 caps.

ACKNOWLEDGMENT

This work was supported by the Research Grants Council of the Hong Kong Special Administrative Region.

[1] C. W. Tang and S. A. Van Slyke, Appl. Phys. Lett. **51**, 913 (1997).
[2] Z. Meng and M. Wong, IEEE Trans. Electron Devices **49**, 991 (2002).
[3] J. Kalinowski, J. Phys. D **32**, R179 (1999).
[4] M. Ikai, S. Tokito, Y. Sakamoto, T. Suzuki, and Y. Taga, Appl. Phys. Lett. **79**, 156 (2001).
[5] H. Aziz, Z. D. Popovic, and N. X. Hu, Appl. Phys. Lett. **81**, 370 (2002).
[6] C. Qiu, H. Chen, M. Wong, and H. S. Kwok, IEEE Trans. Electron Devices **49**, 1540 (2002).
[7] J. M. Bharathan and Y. Yang, J. Appl. Phys. **84**, 3207 (1998).
[8] M. Stossel, J. Staudigel, F. Steuber, J. Simmer, and A. Winnacke, Appl. Phys. A: Mater. Sci. Process. **68**, 387 (1999).
[9] S. C. Kim, S. N. Kwon, M. W. Choi, C. N. Whang, K. Jeong, S. H. Lee, J. G. Lee, and S. Kim, Appl. Phys. Lett. **79**, 3726 (2001).
[10] M. Matsumura, A. Ito, and Y. Miyamae, Appl. Phys. Lett. **75**, 1042 (1999).
[11] L. S. Hung, C. W. Tang, and M. G. Mason, Appl. Phys. Lett. **70**, 152 (1997).
[12] X. Yang, Y. Mo, W. Yang, G. Yu, and Y. Cao, Appl. Phys. Lett. **79**, 563 (2001).
[13] C. C. Wu, C. I. Wu, J. C. Sturm, and A. Kahn, Appl. Phys. Lett. **70**, 1348 (1997).
[14] M. G. Mason, L. S. Hung, C. W. Tang, S. T. Lee, K. W. Wong, and M. Wang, J. Appl. Phys. **86**, 1688 (1999).
[15] S. A. Van Slyke, C. H. Chen, and C. W. Tang, Appl. Phys. Lett. **69**, 2160 (1996).
[16] Y. Shen, D. B. Jacobs, G. G. Malliaras, G. Koley, M. G. Spencer, and A. Ioannidis, Adv. Mater. **13**, 1234 (2001).
[17] C. Qiu, H. Chen, Z. Xie, M. Wong, and H. S. Kwok, Appl. Phys. Lett. **80**, 3485 (2002).
[18] I.-M. Chan, T.-Y. Hsu, and F. C. Hong, Appl. Phys. Lett. **81**, 1899 (2002).

[19] C. Qiu, H. Chen, M. Wong, and H. S. Kwok, IEEE Trans. Electron Devices **48**, 2131 (2001).
[20] S. M. Sze, *Physics of Semiconductor Devices* (Wiley, New York, 1981).
[21] H. Peisert, M. Knupfer, T. Schwieger, and J. Fink, Appl. Phys. Lett. **80**, 2916 (2002).
[22] L. Yan, N. J. Watkins, S. Zorba, Y. Gao, and C. W. Tang, Appl. Phys. Lett. **81**, 2752 (2002).
[23] J. S. Kim, P. K. H. Ho, N. C. Greenham, and R. H. Friend, J. Appl. Phys. **88**, 1073 (2000).
[24] I. D. Parker and H. H. Kim, Appl. Phys. Lett. **64**, 1774 (1994).
[25] H. J. Osten, J. P. Liu, P. Gaworzewski, E. Bugiel, and P. Zaumeil, Tech. Dig. - Int. Electron Devices Meet. , 653 (2002).
[26] S. M. Tracey, A. K. Ray, and T. S. Shishiyanu, IEE Proc.-G: Circuits, Devices Syst. **145**, 383 (1998).